Eur. Phys. J. B (2013) 86: 116
DOI: 10.1140/epjb/e2013-30764-5

THE EUROPEAN PHYSICAL JOURNAL B

Regular Article

Characterization of chaotic maps using the permutation Bandt-Pompe probability distribution

Osvaldo A. Rosso[1,2,3,a], Felipe Olivares[1,4], Luciano Zunino[3,5,6], Luciana De Micco[3,7], André L.L. Aquino[1], Angelo Plastino[3,8,9], and Hilda A. Larrondo[3,7]

[1] LaCCAN/CPMAT – Instituto de Computação, Universidade Federal de Alagoas, BR 104 Norte km 97 57072-970 Maceió, Alagoas, Brazil
[2] Laboratorio de Sistemas Complejos, Facultad de Ingeniería, Universidad de Buenos Aires, 1063 Av. Paseo Colón 840, Ciudad Autónoma de Buenos Aires, Argentina
[3] Fellow of CONICET-Argentina, 1033 Av. Rivadavia 1917, Ciudad Autónoma de Buenos Aires, Argentina
[4] Departamento de Física, Facultad de Ciencias Exactas, Universidad Nacional de La Plata (UNLP), C.C. 67, 1900 La Plata, Argentina
[5] Centro de Investigaciones Ópticas, CIOp (CONICET La Plata - CIC), C.C. 3, 1897 Gonnet, Argentina
[6] Departamento de Ciencias Básicas, Facultad de Ingeniería, Universidad Nacional de La Plata (UNLP), 1900 La Plata, Argentina
[7] Departamentos de Física y de Ingeniería Electrónica, Facultad de Ingeniería, Universidad Nacional de Mar del Plata, Av. Juan B. Justo 4302, 7600 Mar del Plata, Argentina
[8] Instituto de Física, IFLP-CCT, Universidad Nacional de La Plata (UNLP), C.C. 727, 1900 La Plata, Argentina
[9] Instituto de Física Interdisciplinar y Sistemas Complejos, IFISC (CSIC-UIB), Campus Universitat de les Illes Balears, E-07122 Palma de Mallorca, Spain

Received 21 August 2012 / Received in final form 17 December 2012
Published online 27 March 2013 – © EDP Sciences, Società Italiana di Fisica, Springer-Verlag 2013

Abstract. By appealing to a long list of different nonlinear maps we review the characterization of time series arising from chaotic maps. The main tool for this characterization is the permutation Bandt-Pompe probability distribution function. We focus attention on both local and global characteristics of the components of this probability distribution function. We show that forbidden ordinal patterns (local quantifiers) exhibit an exponential growth for pattern-length range $3 \leq D \leq 8$, in the case of finite time series data. Indeed, there is a minimum $D_{\min}$-value such that forbidden patterns cannot appear for $D < D_{\min}$. The system's localization in an entropy-complexity plane (global quantifier) displays typical specific features associated with its dynamics' nature. We conclude that a more "robust" distinction between deterministic and stochastic dynamics is achieved via the present time series' treatment based on the global characteristics of the permutation Bandt-Pompe probability distribution function.

1 Introduction

The study and characterization of time series $\mathcal{S}(t) \equiv \{x_t; t = 1, \ldots, N\}$ by recourse to information theory tools assume that the underlying probability distribution function (PDF) is a priori given. Per contra, part of the concomitant analysis involves extracting the PDF from the data and there is no univocal procedure with which everyone agrees. Bandt and Pompe (BP), almost ten years ago, introduced a successful methodology for the evaluation of the PDF associated to scalar time series data using a symbolization technique [1]. The reader is referred to reference [2] for a didactic description of the approach.

The pertinent symbolic data are (i) created by ranking the values of the series and (ii) defined by reordering the embedded data in ascending order, which is tantamount to a phase space reconstruction with embedding dimension (pattern-length) D and time lag τ (see definitions and methodological details in Ref. [2]). In this way it is possible to quantify the diversity of the ordering symbols (patterns) derived from a scalar time series.

Note that the appropriate symbol-sequence arises naturally from the time series and no model-based assumptions are needed. In fact, the necessary "partitions" are devised by comparing the order of neighboring relative values rather than by apportioning amplitudes according to different levels. This technique, as opposed to most of those in current practice, takes into account the temporal structure of the time series generated by the physical process under study. This feature allows us to uncover important details concerning the ordinal structure of the time series [3–6], and can also yield information about temporal correlation [7,8].

It is clear that this type of analysis of time series entails losing some details of the original series'

[a] e-mail: oarosso@gmail.com

amplitude-information. Nevertheless, by just referring to the series' intrinsic structure, a meaningful difficulty-reduction is indeed achieved by Bandt and Pompe with regards to the description of complex systems. The symbolic representation of time series by recourse to a comparison of consecutive ($\tau = 1$) or non-consecutive ($\tau > 1$) values allows for an accurate empirical reconstruction of the underlying phase-space, even in the presence of weak (observational and dynamical) noise [1]. Furthermore, the ordinal-pattern's associated PDF is invariant with respect to nonlinear monotonous transformations. Accordingly, nonlinear drifts or scalings artificially introduced by a measurement device will not modify the quantifiers' estimation, a nice property if one deals with experimental data (see, i.e., [9]). These advantages make the BP methodology more convenient than conventional methods based on range partitioning.

Additional advantages of the method reside in (i) its simplicity (we need few parameters: the pattern-length/embedding dimension D and the embedding delay τ and (ii) the extremely fast nature of the pertinent calculation-process [10]. The BP methodology can be applied not only to time series representative of low dimensional dynamical systems but also to any type of time series (regular, chaotic, noisy, or reality based). In fact, the existence of an attractor in the D-dimensional phase space is not assumed. The only condition for the applicability of the BP methodology is a very weak stationary assumption (that is, for $k \leq D$, the probability for $x_t < x_{t+k}$ should not depend on t [1]).

The BP-generated probability distribution P is obtained once we choose the embedding dimension D and the embedding delay τ. The former parameter plays an important role in the evaluation of the appropriate probability distribution, since D determines the number of accessible states, given by $D!$. Moreover, it has been established that the length N of the time series must satisfy the condition $N \gg D!$ in order to achieve a reliable statistics and proper distinction between stochastic and deterministic dynamics [3]. With respect to the selection of the parameters, Bandt and Pompe suggest in their cornerstone paper [1] to work with $3 \leq D \leq 7$ with a time lag $\tau = 1$. Nevertheless, other values of τ might provide additional information. Soriano et al. [11,12] and Zunino et al. [13,14], recently showed that when this parameter is relevant, it is strongly correlated with the intrinsic time scales of the system under analysis.

New insight into the characterization of theoretical and observational time series (TS) has been developed via the BP approach in a sensible area, namely, the distinction between chaotic-deterministic and stochastic dynamics. Our present endeavor revolves around this issue. In such a vein,

- Amigó and coworkers considered the emergence of the so-called "forbidden patterns" [5,6], which represents a kind of "particular" feature of some elements of the BP-PDF associated to the TS under study.
- Bandt and Pompe [1] on the one hand, as well as Rosso et al. [3] on the other one, proposed to employ BP-PDFs in order to estimate information theory quantifiers. Examples are the permutation entropy (normalized Shannon one), intensive statistical complexity, and the entropy-complexity plane.

The present work links these two items to show, for finite time series, that even when the presence of forbidden patterns is a characteristic of chaotic dynamics, *a minimum pattern-length*, $D_{\min}$, is necessary in order to detect their presence. This is a fact that has not been previously pointed out in the literature. Ignoring it could be the source of erroneous interpretations. We also show that the number of forbidden patterns, if exist, exhibits, versus the pattern-length D, an exponential behavior, as opposed to the super-exponential behavior described by Amigó and coworkers, valid only for the case $D \to \infty$ [5,6]. Per contra, in the case of quantifiers evaluated making use of the BP-PDF, a specific behavior emerges in the case of chaotic dynamics that provides a more "robust" distinction between deterministic and stochastic dynamics [3,15,16].

The present paper is organized as follows: the methodological framework used in this study is delineated in Section 2 (forbidden and missing ordinal patterns) and in Section 3 (entropy, intensive statistical complexity and entropy-complexity plane). Application to the characterization of chaotic maps and discussion of the pertinent results is the subject of Section 4. Finally, some conclusions are given in Section 5.

2 Forbidden and missing ordinal patterns

As recently shown by Amigó et al. [5,6,17,18], in the case of deterministic chaotic one-dimensional maps not all the possible ordinal patterns can be effectively materialized into orbits, which in a sense makes these patterns "forbidden". In general, one should expect that high-dimensional chaotic dynamical systems (maps) will exhibit forbidden patterns. Indeed, the existence of these *forbidden ordinal patterns* becomes a persistent fact that can be regarded as a "new" dynamical property. Thus, for a fixed pattern-length (embedding dimension D) the number of forbidden patterns of a TS (unobserved patterns) is independent of the series' length N. Remark that this independence is not shared by other properties of the series, such as proximity and correlation, which die out with time [5,6].

Stochastic processes could also display forbidden patterns [15]. However, in the case of either *uncorrelated* (white noise) or *correlated stochastic processes* (noise with power-law spectrum f^{-k} with $k > 0$, fractional Brownian motion and fractional Gaussian noise) it can be numerically ascertained that *no* forbidden patterns emerge. For TS generated by *unconstrained stochastic processes* (uncorrelated processes) every ordinal pattern has the same probability of appearance [5,6,17,18]. Indeed, if the data set is long enough, all ordinal patterns will eventually appear. In this case, as the number of TS-observations increases, the associated PDF becomes uniform, and the number of observed patterns will depend only on the TS-length N.

For correlated stochastic processes the probability of observing a specific individual pattern depends not only on the TS' length N but also on the correlation structure [19]. The existence of a non-observed ordinal pattern does not qualify it as *"forbidden"*, only as *"missing"*, and this could be due to the TS-finite length. A similar observation also holds for the case of real data that always possess a stochastic component due to the omnipresence of dynamical noise [20–22]. Thus, the existence of "missing ordinal patterns" could be either related to stochastic processes (correlated or uncorrelated) or to deterministic noisy processes (always the case for observational time series).

3 Some remarks on Shannon entropy, intensive statistical complexity, and the entropy-complexity plane

It is widely known that an entropic measure does not quantify the degree of structure or patterns present in a process [23]. Moreover, it was recently shown that measures of statistical or structural complexity are necessary for a better understanding of chaotic time series because they are able capture their organizational properties [24]. This specific kind of information is not revealed by randomness' measures. Perfect order (like that of a periodic sequence) and maximal randomness (fair coin toss) possess no complex structure and exhibit zero statistical complexity. For states between these extremes a wide range of possible degrees of structure exists, that should be quantified by an appropriate *statistical complexity measure*.

Rosso and coworkers introduced an effective statistical complexity measure (SCM) that is able to (i) detect essential details of the dynamics and (ii) differentiate between chaos and (different degrees of) periodicity [25]. This specific SCM provides important additional information regarding the peculiarities of the underlying PDF, that is not necessarily detected by the entropy.

The intensive SCM for a given PDF $P = \{p_i \leq 1,\ i = 1, \ldots, M\}$ ($\sum_{i=1}^{M} p_i = 1$) is defined, following the intuitive notion advanced by López-Ruiz et al. [26], via the product

$$\mathcal{C}_{JS}[P] = \mathcal{Q}_J[P, P_e]\mathcal{H}_S[P] \tag{1}$$

of (i) the normalized Shannon entropy [27]

$$\mathcal{H}_S[P] = S[P]/S_{\max}, \tag{2}$$

with $S_{\max} = S[P_e] = \ln M$, $(0 \leq \mathcal{H}_S \leq 1)$ and $P_e = \{1/M, \ldots, 1/M\}$ (the uniform distribution) and (ii) the so-called disequilibrium $\mathcal{Q}_J$. This quantifier is defined in terms of the extensive (in the thermodynamical sense) Jensen-Shannon divergence $\mathcal{J}[P, P_e]$ that links two PDFs. We have

$$\mathcal{Q}_J[P, P_e] = Q_0\mathcal{J}[P, P_e], \tag{3}$$

with

$$\mathcal{J}[P, P_e] = S\left[(P + P_e)/2\right] - S[P]/2 - S[P_e]/2. \tag{4}$$

Q_0 is a normalization constant ($0 \leq \mathcal{Q}_J \leq 1$), equal to the inverse of the maximum possible value of $\mathcal{J}[P, P_e]$. This value is obtained when one of the values of P, say p_m, is equal to one and the remaining p_i values are equal to zero.

The Jensen-Shannon divergence, that quantifies the difference between two (or more) probability distributions, is especially useful to compare the symbol-composition of different sequences [28]. The SCM constructed in this way has the intensive property found in many thermodynamic quantities [25]. We stress the fact that the statistical complexity defined above is the product of two normalized entropies (the Shannon entropy and Jensen-Shannon divergence), but it is a nontrivial function of the entropy because it depends on two different probabilities distributions, i.e., the one corresponding to the state of the system, P, and the uniform distribution, P_e, taken as reference state.

In statistical mechanics one is often interested in isolated systems characterized by an initial, arbitrary, and discrete probability distribution. Evolution towards equilibrium is to be described, as the overriding goal. At equilibrium, we can think, without loss of generality, that this state is given by the uniform distribution P_e. The temporal evolution of the intensive SCM can be analyzed using a diagram of $\mathcal{C}_{JS}$ versus time t. However, it is well known that the second law of thermodynamics states that for isolated systems entropy grows monotonically with time ($d\mathcal{H}_S/dt \geq 0$) [29]. This implies that $\mathcal{H}_S$ can be regarded as an arrow of time, so that an equivalent way to study the temporal evolution of the intensive SCM is through the analysis of $\mathcal{C}_{JS}$ versus $\mathcal{H}_S$. In this way, the normalized entropy-axis substitutes for the time-axis. Furthermore, it has been shown that for a given value of $\mathcal{H}_S$, the range of possible statistical complexity values varies between a minimum $\mathcal{C}_{\min}$ and a maximum $\mathcal{C}_{\max}$ [30], restricting the possible values of the intensive SCM in this plane. Therefore, the evaluation of the complexity provides additional insight into the details of the system's probability distribution, which is not discriminated by randomness measures like the entropy [3,24]. Complexity can also help to uncover information related to the correlational structures related to the components of the physical process under study [7,8]. The entropy-complexity diagram (or plane), $\mathcal{H}_S \times \mathcal{C}_{JS}$, has been used to study changes in the dynamics of a system originated by modifications of some characteristic parameters (see, for instance, Refs. [30–34] and references therein).

4 Characterization of chaotic maps

In the present work, we consider 27 chaotic maps described by Sprott in the appendix of his book [35]. These chaotic maps are grouped as:

a) noninvertible maps: (1) logistic map [36]; (2) sine map [37]; (3) tent map [38]; (4) linear congruential generator [39]; (5) cubic map [40]; (6) Ricker's population model [41]; (7) Gauss map [42]; (8) Cusp map [43]; (9) Pinchers map [44]; (10) Spence map [45]; (11) sine-circle map [46].

b) dissipative maps: (12) Hénon map [47]; (13) Lozi map [48]; (14) delayed logistic map [49]; (15) Tinkerbell map [50]; (16) Burgers' map [51]; (17) Holmes cubic map [52]; (18) dissipative standard map [53]; (19) Ikeda map [54]; (20) Sinai map [55]; (21) discrete predator-prey map [56].

c) conservative maps: (22) Chirikov standard map [57]; (23) Hénon area-preserving quadratic map [58]; (24) Arnold's cat map [59]; (25) Gingerbreadman map [60]; (26) chaotic web map [61]; (27) Lorenz three-dimensional chaotic map [62].

Even when the present list of chaotic maps is not exhaustive, it could be taken as representative of common chaotic systems [35].

For all these chaotic maps we take the same initial conditions and the parameter-values detailed by Sprott. The corresponding initial values are given in the basin of attraction or near the attractor for the dissipative systems, or in the chaotic sea for the conservative systems [35]. For each map's TS-generation we discarded the first 10^5 iterations and, after that, N iterations-data were generated. The BP-PDF was evaluated for each time series of N data with pattern-lengths $3 \leq D \leq 8$ with $\Delta D = 1$ and time lag $\tau = 1$.

For multi-dimensional maps each of the pertinent coordinates is not independent by itself and the associated TS (one-dimensional TS) carries information about the complete dynamical system. In fact, one can use any of these associated TS for evaluating the dynamical system's invariants (like correlation dimension, Lyapunov exponents, etc.), by appealing to a time lag reconstruction [35]. In the present work, we analyze TS generated by each one of chaotic map coordinates, when the corresponding map is bi- or multi-dimensional. Due to the fact that the BP-PDF is not a dynamical invariant (neither are other quantifiers derived by information theory) some variation could be expected in the quantifiers' values computed with this PDF, whenever one or other of the TS generated by these multidimensional coordinate systems.

Chaotic TS display forbidden ordinal patterns as mentioned earlier [5]. However, failing to observe a given specific ordinal pattern in a TS does not necessarily imply that this pattern is forbidden. Its absence qualifies the pattern just as a missing one. This could happen because the pertinent TS is not long enough. In practice, we can say that the observation or not of an ordinal pattern will depend strongly on the TS-length N. Thus, if the number of non-observed ordinal patterns is constant for increasing values of the time series N, one can speak of "true" forbidden ordinal patterns. In the following, for our analysis of forbidden ordinal patterns, we will consider a TS length of $N = 10^n$ data, with $3 \leq n \leq 7$ and $\Delta n = 1$.

We study the forbidden/missing ordinal patterns, in the 27 chaotic TS under analysis, as a function of (i) the TS-length N and (ii) the embedding dimension (pattern-length) D. A rather interesting result ensues: depending on the chaotic map analyzed, a minimum pattern-length (denoted by $D_{\min}$) is found for which the existence of forbidden ordinal patterns will indeed be detected.

The corresponding chaotic maps and the associated values of $D_{\min}$, for the maximum TS length $N = 10^7$ data, are:

- $D_{\min} = 3$: logistic map; sine map; tent map; Ricker's population map; Cusp map; Pinchers map; Spence map; Hénon map; Lozi map.
- $D_{\min} = 4$: sine-circle map; delay logistic map; Tinkerbell map; Burgers' map; discrete predator-prey map; Chirikov standard map; Hénon area-preserving quadratic map; Gingerbreadman map; chaotic web map.
- $D_{\min} = 5$: cubic map; Holmes cubic map; Ikeda map; Lorenz three-dimensional chaotic map.
- $D_{\min} = 6$: Sinai map; Arnold's map.
- $D_{\min} = 7$: linear congruential generator.
- $D_{\min} = 8$: Gauss map; dissipative standard map (X).

For dissipative standard maps (Y), no forbidden/missing patterns are observed for all (i) TS lengths considered ($n \leq 7$) and (ii) embedding dimensions D, so that we can assume that $D_{\min} > 8$.

Amigó and coworkers remark that "true forbidden patterns in deterministic sequences (time series) have two basic properties: (i) robustness against observational noise and (ii) super-exponential growth with the length" [18]. The last property is proved by the authors (i) in the case $D \to \infty$ and (ii) also assuming enough TS data, $N \to \infty$. We have analyzed the behavior of the estimated number of forbidden patterns (denoted by N^*) as a function of the patterns-length D in order to establish which is the related behavior in a more practical context (TS with finite number N of data and pattern-length D not higher than 8).

We propose to fit $\ln N^*$ by a linear (exponential growth) or by a nonlinear dependence (super exponential growth) with D [63]. For the corresponding analysis we consider $D_{\min} \leq D \leq 8$, $\Delta D = 1$, $N = 10^7$ data (initial conditions given by Sprott [35]). We have excluded from this analysis those chaotic maps for which $D_{\min} \geq 8$ in order to have at least two points in the fit range. More precisely, the Gauss and the dissipative standard maps are not considered.

In Figure 1, the values corresponding to $\ln N^*$ vs. D are displayed for the three kinds of maps mentioned above: noninvertible, dissipative and conservative. A linear fit $\ln N^* = \alpha_0 + \alpha_1 D$ is proposed. From the results obtained for each one of these 25 maps: parameter values $\alpha_{0,1}$ (plus associated standard errors), fit value R and, usual analysis of residual, no structural details are revealed; leading one to conclude that the proposed linear approach provides a very good description. Summarizing over these chaotic maps, for the parameter α_1 we obtain (average values and standard deviation) $\langle \alpha_1 \rangle = 2.31 \pm 0.53$ and the goodness coefficient is $\langle R \rangle = 0.99496 \pm 0.01082$. Consequently, we gather that in a practical context (N finite and $D \leq 8$) the behavior of the observed number of forbidden/missing patterns N^* grows *exponentially* with the pattern-length D.

Figure 2 displays, for all the 27 chaotic maps here considered, the entropy-complexity plane $\mathcal{H}_S \times \mathcal{C}_{JS}$ location.

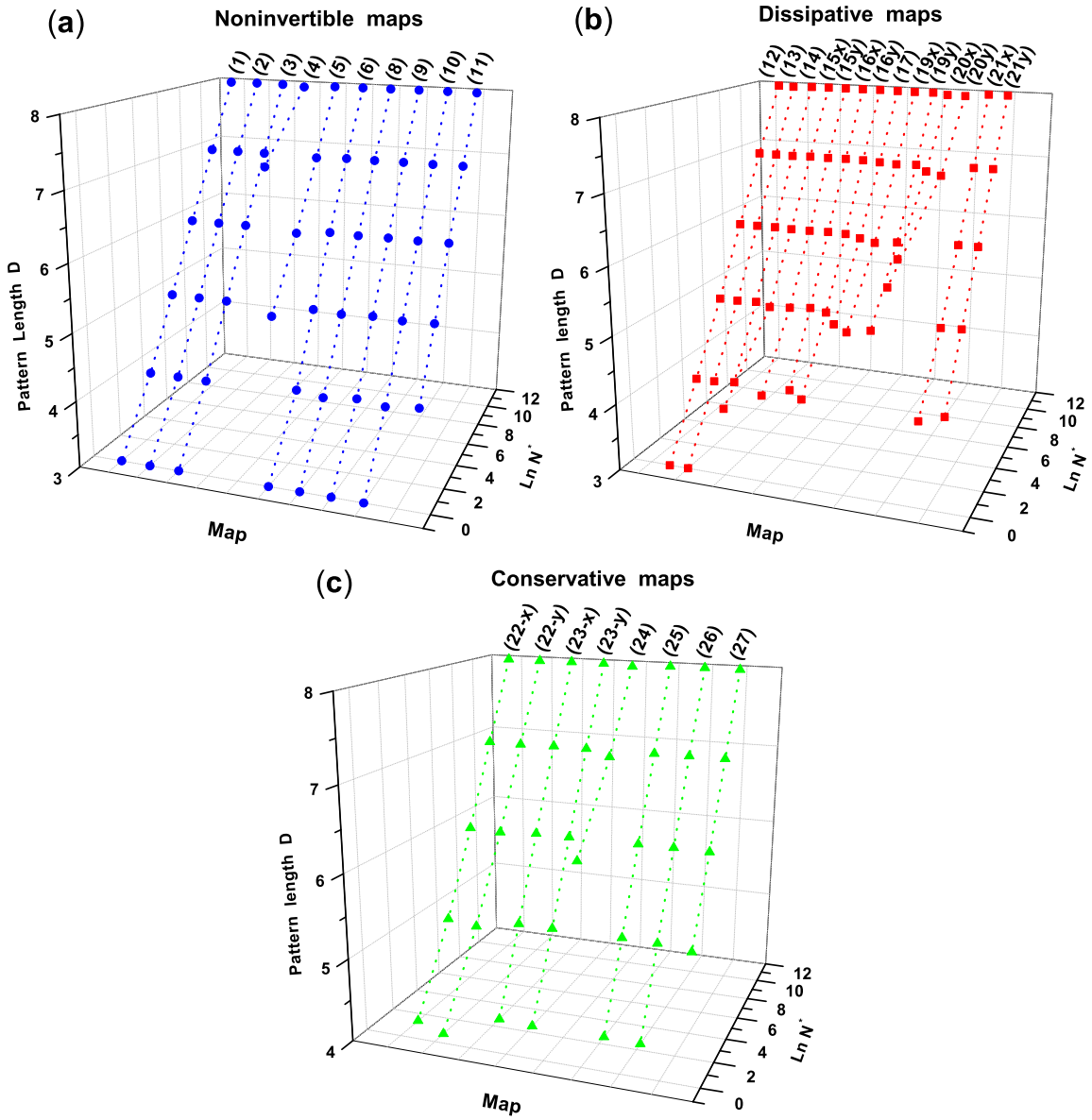

Fig. 1. Dependence of the number of forbidden patterns $\ln N^*$ as a function of the pattern-length D for the three kinds of maps: (a) noninvertible, (b) dissipative and, (c) conservative. Time series with $N = 10^7$ data (initial conditions given by Sprott [35]) were considered. The pattern-lengths considered were $D_{\min} \leq D \leq 8$ and only chaotic maps with $D_{\min} \leq 7$ in order to have at least two points in the fit range. The numbers between parentheses represent the corresponding chaotic map enumerated at the beginning of Section 4. The letters "X" and "Y" represent the TS coordinates maps for which their $\ln N^*$-values are clearly distinguishable.

The BP-PDF is evaluated for $D = 6$, $\tau = 1$, and a TS-length $N = 10^7$ data (for initial conditions given by Sprott [35]). In this graph, the given numbers represent the chaotic maps enumerated at the beginning of this section. The letters "X" and "Y" represent the TS coordinates maps, for which their planar representations are displayed. We also present in this plot the planar localization for a stochastic process: noises with f^{-k} power spectrum [64] ($0 \leq k \leq 3.5$, with $\Delta k = 0.25$). The corresponding values for these noises represent the average value for ten realizations ($N = 10^6$ data), generated with different seeds.

As a general behavior, all points corresponding to the 27 chaotic maps are found in close vicinity to the maximum complexity curve $\mathcal{C}_{\max}$. In particular, for the case of chaotic maps with $3 \leq D_{\min} \leq 5$, they are localized at a region of intermediate normalized Shannon entropy $\mathcal{H}_S$ and high intensive statistical complexity $\mathcal{C}_{JS}$ (close to the curve of maximum complexity), in agreement with previously published results (see Fig. 1 in Ref. [3]). Interestingly enough, localization in the entropy-complexity plane for chaotic maps with $D_{\min} \geq 6$ tends to follow a similar behavior, that is, high values of complexity but now with $\mathcal{H}_S \geq 0.9$.

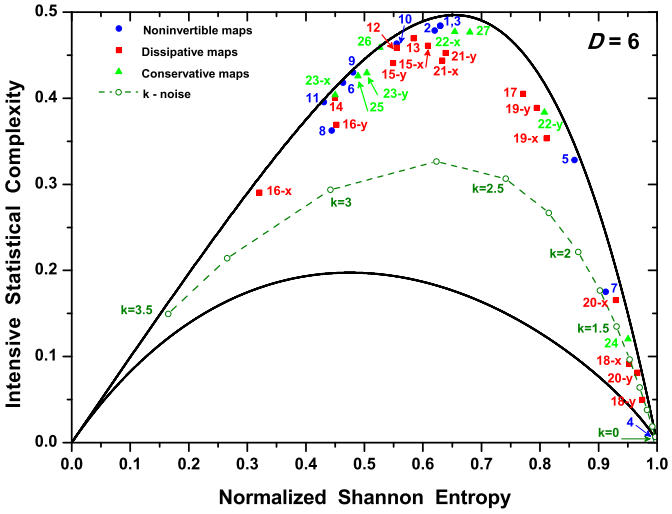

Fig. 2. Localization in the entropy-complexity plane of the 27 chaotic maps considered in the present work. The Bandt-Pompe PDF was evaluated considering $D = 6$ (pattern-length), $\tau = 1$ (time lag) and time series length $N = 10^7$ data (initial conditions given by Sprott [35]). The inside numbers represent the corresponding chaotic map enumerated at the beginning of Section 4. The letters "X" and "Y" represent the TS coordinates maps for which their planar representation is clearly distinguishable. The open circle-dash line represents the planar localization (average values over ten realizations with different seeds) for the stochastic process: noises with f^{-k} power spectrum. The continuous lines represent the curves of maximum and minimum statistical complexity, $\mathcal{C}_{\max}$ and $\mathcal{C}_{\min}$, respectively, as functions of the normalized Shannon entropy [30].

For stochastic process noises with f^{-k} power spectrum, the localization in the plane $\mathcal{H}_S \times \mathcal{C}_{JS}$ exhibits a decreasing entropic behavior ranging from $\mathcal{H}_S \sim 1$ for $k = 0$ to $\mathcal{H}_S \sim 0.15$ for $k = 3.5$ (see Fig. 2). Note that, for the case of $k = 0$, uncorrelated non-Gaussian noise, it location closely approaches the extreme value $(\mathcal{H}_S, \mathcal{C}_{JS}) = (1, 0)$. For $k > 0$, correlated non-Gaussian noises (colored noises) display lower entropic values. The associated statistical complexity values, that belong to the interval $0 \leq \mathcal{C}_{JS} \leq 0.35$, range in-between the extreme complexity values $\mathcal{C}_{\min}$ and $\mathcal{C}_{\max}$ (see Fig. 2). Similar planar behavior is observed for fractional Brownian motion (fBm) and fractional Gaussian noise (fGn) stochastic processes (see Fig. 1 in Ref. [3]).

Summing up, Figure 2 illustrates the clear difference in planar location between a chaotic maps (deterministic dynamics) and stochastic processes. Moreover, a similar behavior is obtained when the analysis is performed for other D-values.

In the following, and without loss of generality, we give a more detailed results-discussion for the following six chaotic maps.

1. *Logistic map* [36]:

$$X_{n+1} = A\ X_n(1 - X_n) \tag{5}$$

Parameter value: $A = 4$; initial condition: $X_0 = 0.1$; Lyapunov exponent: $\lambda = \ln 2 = 0.693147181\ldots$

2. *Linear congruential generator* [39]:

$$X_{n+1} = A\ X_n + B \qquad (\text{Mod } C) \tag{6}$$

Parameter values: $A = 7141$, $B = 54773$, $C = 259200$; initial condition: $X_0 = 0$; Lyapunov exponent: $\lambda = \ln|A| = 8.873608101\ldots$

3. *Gauss map* [42]:

$$X_{n+1} = 1/X_n \qquad (\text{Mod } 1) \tag{7}$$

Initial condition: $X_0 = 0.1$; Lyapunov exponent: $\lambda \simeq 2.373445$.

4. *Dissipative standard map* [53]:

$$\begin{cases} X_{n+1} = X_n + Y_{n+1} & (\text{Mod } 2\pi) \\ Y_{n+1} = b\ Y_n + k\ \sin(X_n) & (\text{Mod } 2\pi) \end{cases} \tag{8}$$

Parameter values: $b = 0.1$, $k = 8.8$; initial conditions: $X_0 = 0.1$, $Y_0 = 0.1$; Lyapunov exponents: $\lambda_1 \simeq 1.46995$, $\lambda_2 \simeq -3.77254$.

5. *Sinai map* [55]:

$$\begin{cases} X_{n+1} = X_n + Y_n + \delta\ \cos(2\pi Y_n) & (\text{Mod } 1) \\ Y_{n+1} = X_n + 2\ Y_n & (\text{Mod } 1) \end{cases} \tag{9}$$

Parameter value: $\delta = 0.1$; initial conditions: $X_0 = 0.5$, $Y_0 = 0.5$; Lyapunov exponents: $\lambda_1 \simeq 0.95946$, $\lambda_2 \simeq -1.07714$.

6. *Arnold's cat map* [59]:

$$\begin{cases} X_{n+1} = X_n + Y_n & (\text{Mod } 1) \\ Y_{n+1} = X_n + k\ Y_n & (\text{Mod } 1) \end{cases} \tag{10}$$

Parameter value: $k = 2$; initial conditions: $X_0 = 0$, $Y_0 = 1/\sqrt{2}$; Lyapunov exponents: $\lambda_{1,2} = \pm\ln[\frac{1}{2}(3 + \sqrt{5})] = \pm 0.96242365\ldots$

The first one is representative of maps with low $D_{\min}$ while for the remaining maps, a high $D_{\min}$-value is required. Note also that the first three are one-dimensional maps while the next three maps are bi-dimensional ones. Figure 3 displays X_{n+1} versus X_n for the one-dimensional maps and Y_n versus X_n for the bi-dimensional ones. Note that a clearly outlined structure is observed for the case of the logistic, Gauss, and Dissipative standard maps. From these graphs (Fig. 3), one can observe also that the linear congruential generator, the Arnold's cat map, and the Sinai map, cover the bi-dimensional space in an almost homogeneous way in the case of the first two maps, and with some degree of structure insinuating itself in the last one.

The average number (standard deviation) of observed forbidden/missing ordinal patterns as a function of (i) the time series length $N = 10^n$ data ($3 \leq n \leq 7$,

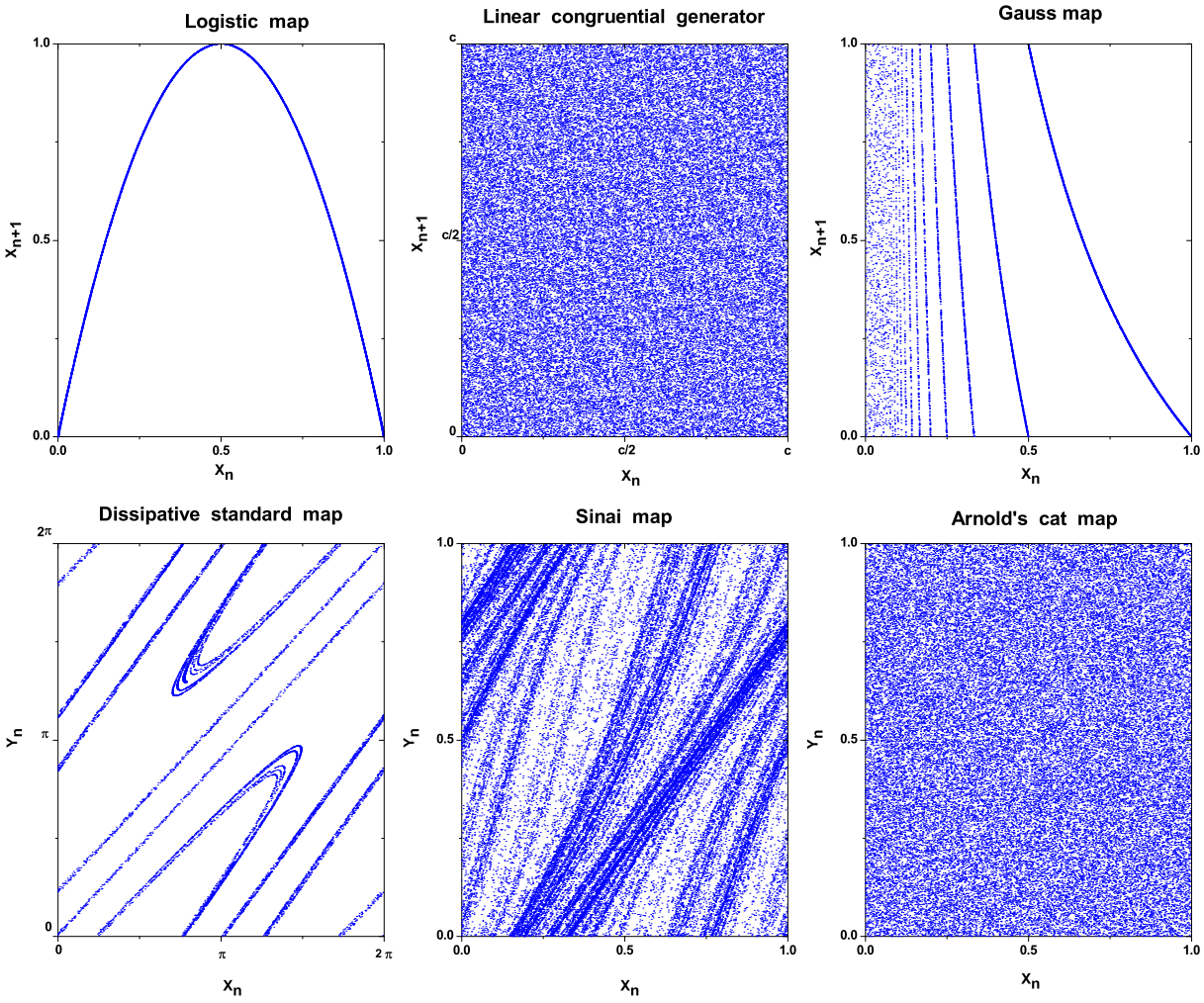

Fig. 3. Graphical representation for the 6 chaotic maps (initial conditions given by Sprott [35]) analyzed with more detail in the text. The graphs display X_{n+1} versus X_n for the one-dimensional maps: logistic, linear congruential generator, and Gauss, on the one hand, and Y_n versus X_n for the bi-dimensional maps: dissipative standard, Sinai, and Arnold's cat, on the other hand.

$\Delta n = 1$); (ii) the pattern-length (embedding dimension) D ($3 \leq D \leq 8$, $\Delta D = 1$), time lag $\tau = 1$; (for ten different initial conditions) are listed in Table 1 for the above six chaotic maps. In the case of bi-dimensional chaotic maps, the values for each one of the map's coordinates are detailed.

As expected, the results displayed in Table 1 do not depend (zero standard deviation) on the chaotic map's initial conditions, if the true number of forbidden patterns can be detected for the time series' length considered. If such conditions are not fulfilled for the maximum TS-lengths considered, we also notice in Table 1 an overestimation of the number of forbidden ordinal patterns (some of them are missing patterns). However, the corresponding standard error is quite low compared with the mean value, allowing us to take the numerical mean value $\langle N^* \rangle$ as representative of the number of forbidden ordinal patterns characterizing the chaotic map.

In the case of the logistic map, inspection of Table 1 makes it clear that forbidden ordinal patterns are observed for all the pattern-lengths here considered. Thus, for this map one has $D_{\min} = 3$. Note also that values of forbidden ordinal patterns N^* are stable (constant, with zero standard deviation) for most of the different time series lengths considered by us. For the conjunction $X_0 = 0.1$, $D = 7$ and $N = 10^3$, we detect $N^* = 4866$ forbidden/missing patterns (some of these do not appear due to the short length of the pertinent time series), which reduces to $N^* = 4862$ forbidden patterns with zero standard deviation for TS-lengths with $N = 10^4$ up to 10^7 data. In this last case, such is the number of real forbidden patterns. Note also the exponential growth of forbidden ordinal patterns for increasing values of the pattern-length D (see Fig. 1a). A similar situation is also observed for the rest of our chaotic maps.

Table 1 allows one to conclude that the number of missing ordinal patterns tends to vanish as the time series' length grows, if the pattern-length considered is $D < D_{\min}$. We only start to find a non-zero number of forbidden/missing ordinal patterns when considering

Table 1. Mean value of number of forbidden/missing ordinal patterns (standard deviation) for 10 different initial conditions, as a function of the chaotic time series length N for pattern-length D corresponding to the six chaotic maps analyzed with more detail in the text.

Map			Forbidden/missing patterns (mean value and standard deviation)					
	Lyapunov	10^n *data*	$D=3$	$D=4$	$D=5$	$D=6$	$D=7$	$D=8$
Logistic map	$\lambda = \ln 2$	3	1	12	89	645.10	4869.90	39981.80
	$= 0.693147\ldots$		(0)	(0)	(0)	(0.32)	(2.42)	(8.48)
		4	1	12	89	645	4862	39906.80
			(0)	(0)	(0)	(0)	(0)	(0.92)
		5	1	12	89	645	4862	39906
			(0)	(0)	(0)	(0)	(0)	(0)
		6	1	12	89	645	4862	39906
			(0)	(0)	(0)	(0)	(0)	(0)
		7	1	12	89	645	4862	39906
			(0)	(0)	(0)	(0)	(0)	(0)
Lineal congruential	$\lambda = \ln \lvert A \rvert$	3	0	0	0	167.10	4144.30	39344.20
generator	$= 8.873608\ldots$		(0)	(0)	(0)	(9.46)	(11.07)	(3.68)
		4	0	0	0	0	1182	32518.20
			(0)	(0)	(0)	(0)	(13.71)	(44.39)
		5	0	0	0	0	341.80	23448.40
			(0)	(0)	(0)	(0)	(3.12)	(38.91)
		6	0	0	0	0	279	21895
			(0)	(0)	(0)	(0)	(0)	(0)
		7	0	0	0	0	279	21895
			(0)	(0)	(0)	(0)	(0)	(0)
Gauss map	$\lambda \simeq 2.373445$	3	0	0	4.80	330	4323.10	39420
			(0)	(0)	(1.69)	(19.75)	(26.30)	(16.63)
		4	0	0	0	31.50	2305.60	34421.60
			(0)	(0)	(0)	(6.65)	(41.01)	(85.32)
		5	0	0	0	0	340.70	20292
			(0)	(0)	(0)	(0)	(20.59)	(98.31)
		6	0	0	0	0	1	4779.70
			(0)	(0)	(0)	(0)	(0.82)	(41.51)
		7	0	0	0	0	0	121
			(0)	(0)	(0)	(0)	(0)	(7.51)
Dissipative standard	$\lambda_1 \simeq 1.46995$	3	0	0	0.80	257.80	4252.80	39398.90
map (X)	$\lambda_2 \simeq -3.77254$		(0)	(0)	(0.92)	(16.40)	(23.05)	(16.07)
		4	0	0	0	4.60	1578.20	33464.20
			(0)	(0)	(0)	(2.80)	(36.66)	(83.29)
		5	0	0	0	0	35.50	13336.50
			(0)	(0)	(0)	(0)	(5.60)	(166.79)
		6	0	0	0	0	0	871.50
			(0)	(0)	(0)	(0)	(0)	(27.73)
		7	0	0	0	0	0	28.90
			(0)	(0)	(0)	(0)	(0)	(4.07)
Dissipative standard	$\lambda_1 \simeq 1.46995$	3	0	0	0.10	223.90	4201.40	39364.80
map (Y)	$\lambda_2 \simeq -3.77254$		(0)	(0)	(0.32)	(12.81)	(10.20)	(8.10)
		4	0	0	0	0	1130.90	32550.70
			(0)	(0)	(0)	(0)	(52.30)	(108.68)
		5	0	0	0	0	1.20	7837.20
			(0)	(0)	(0)	(0)	(1.23)	(86.93)
		6	0	0	0	0	0	3
			(0)	(0)	(0)	(0)	(0)	(1.56)
		7	0	0	0	0	0	0
			(0)	(0)	(0)	(0)	(0)	(0)

Table 1. continued.

Map			Forbidden/missing patterns (mean value and standard deviation)					
	Lyapunov	10^n *data*	$D=3$	$D=4$	$D=5$	$D=6$	$D=7$	$D=8$
Sinai map (X)	$\lambda_1 \simeq 0.95946$	3	0	0	6	316.60	4284.90	39399.50
	$\lambda_2 \simeq -1.07714$		(0)	(0)	(1.63)	(13.76)	(22.54)	(15.51)
		4	0	0	1.10	92	2483.30	34336.30
			(0)	(0)	(0.32)	(5.03)	(29.86)	(66.21)
		5	0	0	0.70	48.10	1499.10	25928.70
			(0)	(0)	(0.48)	(2.42)	(12.51)	(34.28)
		6	0	0	0	37.30	1228.20	21739.80
			(0)	(0)	(0)	(1.06)	(6.84)	(18.95)
		7	0	0	0	34	1149.80	20360.40
			(0)	(0)	(0)	(0)	(4.44)	(9.02)
Sinai map (Y)	$\lambda_1 \simeq 0.95946$	3	0	0	0.30	246.80	4223.50	39377.30
	$\lambda_2 \simeq -1.07714$		(0)	(0)	(0.48)	(11.59)	(16.83)	(11.20)
		4	0	0	0	22.60	2031	33856.60
			(0)	(0)	(0)	(3.86)	(36.11)	(59.31)
		5	0	0	0	4.30	894.90	23529.50
			(0)	(0)	(0)	(1.25)	(10.46)	(42.49)
		6	0	0	0	1.10	653.70	18621
			(0)	(0)	(0)	(0.32)	(3.89)	(17.51)
		7	0	0	0	1	585.10	17107.80
			(0)	(0)	(0)	(0)	(2.58)	(22.71)
Arnold's map (X)	$\lambda_1 = 0.962423\ldots$	3	0	0	1.80	276.90	4254.50	39384
	$\lambda_2 = -0.962423\ldots$		(0)	(0)	(1.78)	(8.16)	(12.53)	(9.19)
		4	0	0	0	57.20	2330.30	34149.70
			(0)	(0)	(0)	(2.66)	(25.50)	(42.62)
		5	0	0	0	32.10	1434.80	25726.50
			(0)	(0)	(0)	(0.32)	(9.87)	(41.79)
		6	0	0	0	32	1287.60	22713.80
			(0)	(0)	(0)	(0)	(0.97)	(16.57)
		7	0	0	0	32	1284	22149.90
			(0)	(0)	(0)	(0)	(0)	(3.54)
Arnold's map (Y)	$\lambda_1 = 0.962423\ldots$	3	0	0	1.80	280.90	4256.30	39389.60
	$\lambda_2 = -0.962423\ldots$		(0)	(0)	(1.14)	(10.27)	(18.40)	(14.47)
		4	0	0	0	57.20	2329.40	34153
			(0)	(0)	(0)	(4.42)	(18.07)	(49.42)
		5	0	0	0	32.20	1430.20	25684
			(0)	(0)	(0)	(0.42)	(7.89)	(33.20)
		6	0	0	0	32	1287.30	22711
			(0)	(0)	(0)	(0)	(1.89)	(12.50)
		7	0	0	0	32	1284	22152
			(0)	(0)	(0)	(0)	(0)	(3.86)

pattern-lengths $D \geq D_{\min}$. We also observe (see Tab. 1) that the total number of forbidden/missing patterns tends to stabilize itself as the length of the series increases, suggesting that this number is indeed the genuine, actual one. In the case of the dissipative standard map (Y), zero missing patterns are observed for pattern-length $D = 8$ together with $N = 10^7$ data, indicating that for this chaotic map the minimum pattern-length $D_{\min} > 8$.

Continuing with the six chaotic maps' TS with $N = 10^7$ data mentioned above, Figure 4 displays the results for BP-PDFs corresponding to $D = 6$ and $\tau = 1$. The number of observed forbidden patterns is also given (initial conditions given by Sprott [35]) inside each figure. The BP-PDF for the logistic map and the one corresponding to the linear congruential generator, represent the extreme cases of PDFs far away from and close to, respectively, the uniform one. These BP-PDFs constitute invariant PDFs for the corresponding maps. Pay attention now to the sample $\mathbf{x}$ of N observations. By the law of large numbers, the sample quantity $\Psi(\mathbf{x})$ converges in probability to its distributional counterpart as the sample size N increases (see, for instance, Refs. [65,66]). Accordingly, quantifiers like

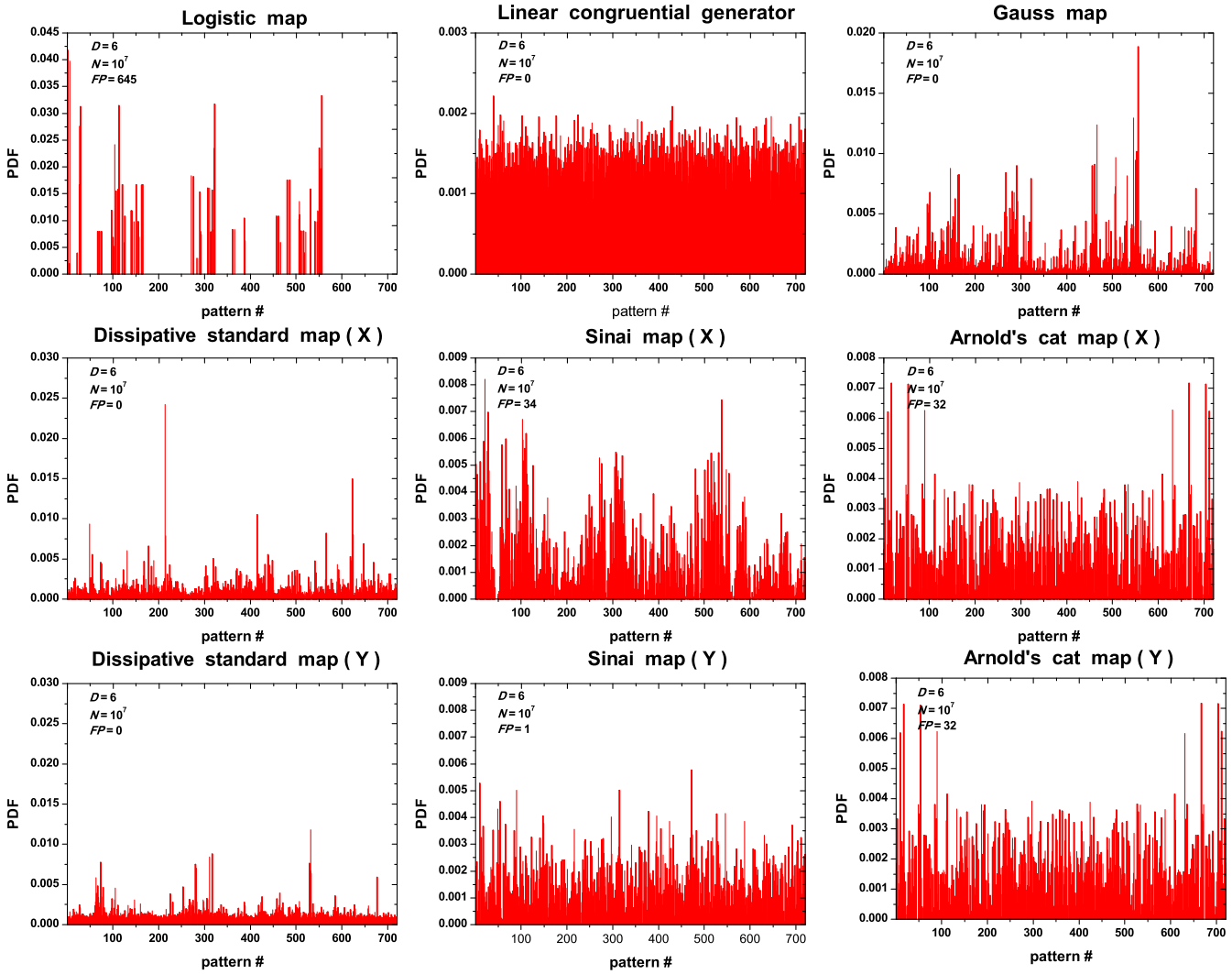

Fig. 4. The Bandt-Pompe PDF for the chaotic maps considered in detail the present work, for the case $D = 6$ (pattern length) and $\tau = 1$ (time lag) with a time series containing $N = 10^7$ data. The number of forbidden/missing patterns (FP) is also reported inside each figure. The letters "X" and "Y" represent the TS coordinates maps.

entropies and complexities (divergences) will be as accurate indicators as one wishes, whenever an adequate sample's size is provided. Thus, we are able to (i) use our BP-PDF for evaluating specific information theory based quantifiers (like a normalized Shannon entropy and an intensive statistical complexity) and (ii) regard these tools as global quantifiers of the chaotic dynamics under study.

See in Figure 5, for the six chaotic maps mentioned above (initial conditions given by Sprott [35]), the estimated values for the normalized Shannon entropy $\mathcal{H}_S$ and intensive statistical complexity $\mathcal{C}_{JS}$, as functions of the TS-length n ($N = 10^n$, $3 \leq n \leq 8$, $\Delta n = 1$). The corresponding map quantifiers are evaluated via the BP-PDF, with $D = 6$ and $\tau = 1$. Note how the pertinent values tend to stabilize themselves as the TS-length increases, reaching in all the cases, in a rather fast fashion, a plateau. The invariant expected behavior of these BP-PDFs is clearly observed in this graph.

The location in the entropy-complexity plane of chaotic maps with $D_{\min} \geq 6$ tends to follow a behavior similar to the ones discussed earlier (maps with $3 \leq D_{\min} \leq 5$), that is, high values of complexity close to the curve of maximum complexity but now with $\mathcal{H}_S \geq 0.9$, as can be appreciated in Figure 6. Planar locations for noises with f^{-k} power spectrum are also displayed. One can see that the chaotic maps exhibit planar localization that lie on top of those belonging to stochastic processes, except for the dissipative standard map, which lies a little below. The location in the entropy-complexity plane of the linear congruential generator constitutes the extreme case (see Fig. 6). The planar position of this chaotic map, when the triplet $D = 6$, $\tau = 1$, $N = 10^7$ data is used, is the point $(0.997871, 0.005101)$, very close to the curve $\mathcal{C}_{\max}$ in $\mathcal{H}_S \times \mathcal{C}_{JS}$. For comparison's sake we indicate the planar position attained by both (i) pure non-Gaussian and (ii) Gaussian white noises. These locations are given by

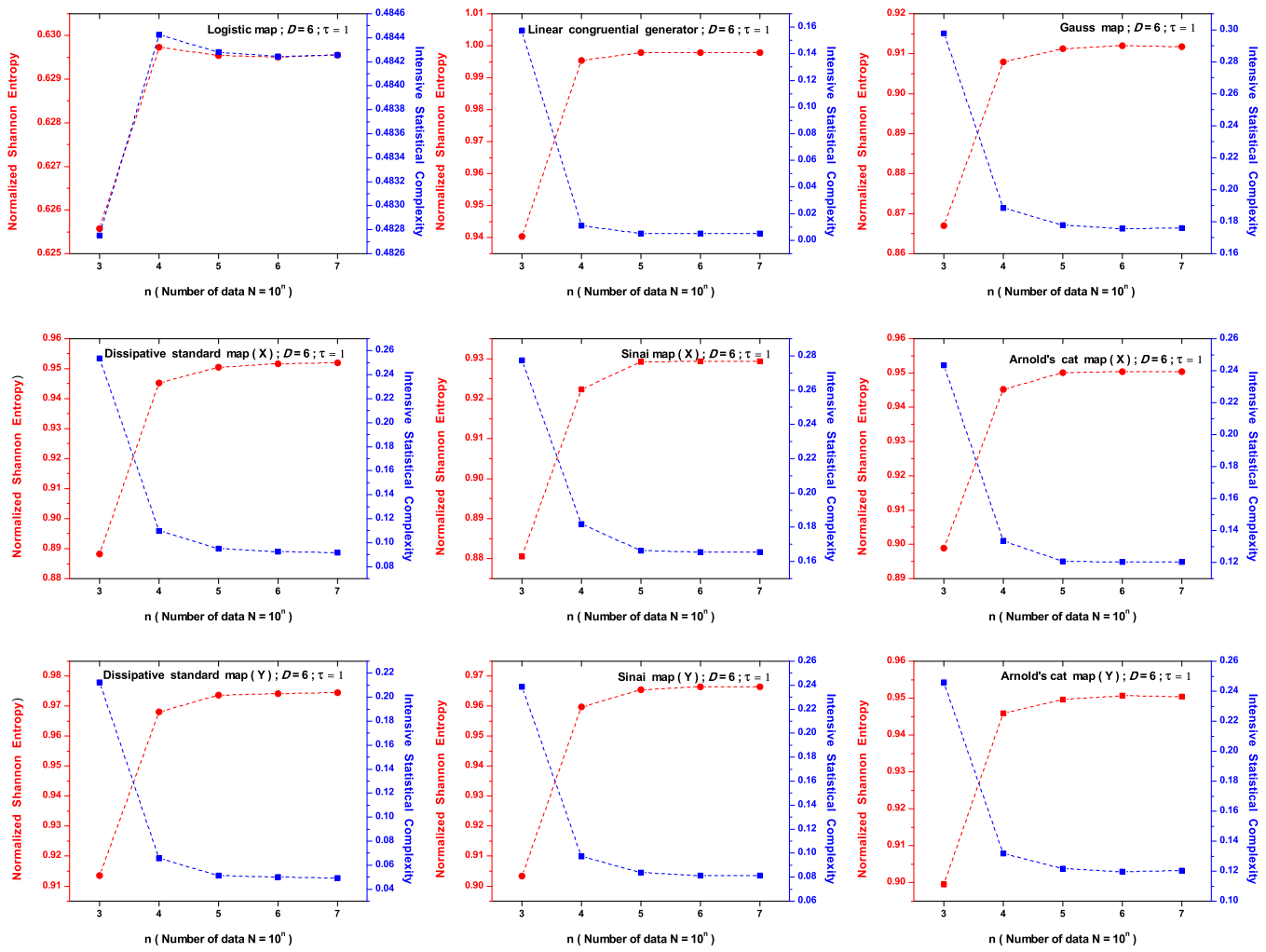

Fig. 5. Variation of the information theory quantifiers, normalized Shannon entropy ($\mathcal{H}$) and intensive statistical complexity ($\mathcal{C}$) as a function of the time series length $N = 10^n$ ($3 \leq n \leq 7$), evaluated with PDF-Bandt and Pompe, with $D = 6$ and $\tau = 1$, for the six chaotic maps analyzed with more detail in the text. The letters "X" and "Y" represent the TS coordinates maps.

the points $(0.999943, 0.000134)$ and $(0.999945, 0.000130)$, respectively. We note a clear difference between the planar localization of either a chaotic map or a stochastic process.

5 Conclusions

We reviewed in the present work the characterization of some chaotic maps' TS from the viewpoint of the permutation Bandt-Pompe PDFs. We considered "local" characteristics of the components of this PDF, the so-called forbidden/missing ordinal patterns, as well as quantifiers derived from information theory (normalized Shannon entropy, intensive statistical complexity, entropy-complexity plane) that make use of all the components of the PDF, and are accordingly called "global".

If forbidden ordinal patterns are observed in a finite data time series, they exhibit an exponential growth for finite pattern-lengths (embedding dimension) D. This behavior could be regarded as the hallmark of determinism in a time series. We have shown that even when the presence of forbidden patterns can be associated to a chaotic dynamics, a minimum pattern-length, $D_{\min}$ must be considered in order to observe this phenomenon. This is a fact that has not been pointed out before. In fact, we could not find any reference to $D_{\min}$ in the published literature. Moreover, we infer from it that, using the Band-Pompe methodology, the existence of this quantity was not considered in classifying time series as either deterministic or stochastic. Note that ignoring the existence (discovered by us here) of this minimal pattern-length could lead to wrong interpretations.

Per contra, in the case of quantifiers evaluated making use of the whole BP-PDF, for fixed values of the pattern-length (embedding dimension) D and time lag τ, a specific behavior is observed for the case of chaotic dynamics. Localization in the entropy-complexity plane $\mathcal{H}_S \times \mathcal{C}_{JS}$, for the case of chaotic maps, closely approaches the limiting curve of maximum statistical complexity $\mathcal{C}_{\max}$. Note that a similar behavior is still observed when chaotic maps' TS are contaminated with small or moderate amount of

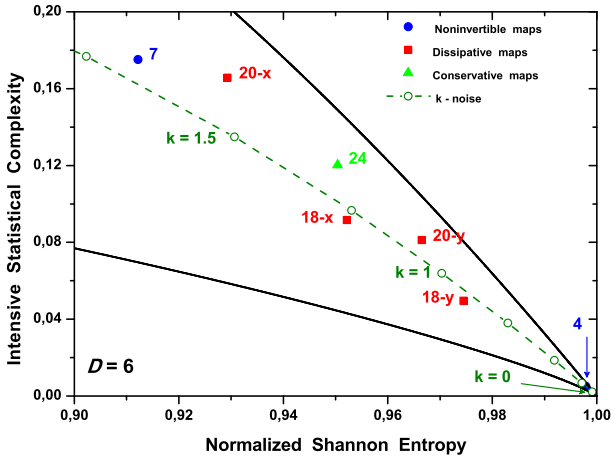

Fig. 6. Localization in the entropy-complexity plane of the 6 chaotic maps (initial conditions given by Sprott [35]) analyzed with more detail in the text. The Bandt-Pompe PDF was evaluated considering $D = 6$ (pattern-length), $\tau = 1$ (time lag) and TS-length $N = 10^7$ data. The inside numbers represent the corresponding chaotic map enumerated at the beginning of Section 4. The letters "X" and "Y" represent the TS coordinates maps for which their planar representation is clearly distinguishable. The open circle-dash line represents the planar localization (average values over ten realizations with different seeds) for the stochastic process: noises with f^{-k} power spectrum. The continuous lines represent the curves of maximum and minimum statistical complexity, $\mathcal{C}_{\max}$ and $\mathcal{C}_{\min}$, respectively, as functions of the normalized Shannon entropy [30].

additive uncorrelated or correlated noise [15,16]. Based on such behavior, we conclude that a more "robust" distinction between deterministic and stochastic dynamics is given via the present TS-treatment, that takes into account the whole of the permutation Bandt-Pompe PDF (global quantifier), and not just part of it.

O.A. Rosso gratefully acknowledges support from CNPq, Fellowship, Brazil. F. Olivares is supported by a Fellowship of the Chilean Government, CONICYT. This work was partially supported by the projects PIP1177 and PIP112-200801-01420 of CONICET (Argentina), and the projects FIS2008-00781/FIS (MICINN)-FEDER (EU) (Spain, EU).

References

1. C. Bandt, B. Pompe, Phys. Rev. Lett. **88**, 174102 (2002)
2. M. Zanin, L. Zunino, O.A. Rosso, D. Papo, Entropy **14**, 1553 (2012)
3. O.A. Rosso, H.A. Larrondo, M.T. Martín, A. Plastino, M.A. Fuentes, Phys. Rev. Lett. **99**, 154102 (2007)
4. M. Zanin, Chaos **18**, 013119 (2008)
5. J.M. Amigó, S. Zambrano, M.A.F. Sanjuán, Europhys. Lett. **79**, 50001 (2007)
6. J.M. Amigó, *Permutation complexity in dynamical systems* (Springer-Verlag, Berlin, 2010)
7. O.A. Rosso, C. Masoller, Phys. Rev. E **79**, 040106(R) (2009)
8. O.A. Rosso, C. Masoller, Eur. Phys. J. B **69**, 37 (2009)
9. P.M. Saco, L.C. Carpi, A. Figliola, E. Serrano, O.A. Rosso, Physica A **389**, 5022 (2010)
10. K. Keller, M. Sinn, Physica A **356**, 114 (2005)
11. M.C. Soriano, L. Zunino, L. Larger, I. Fischer, C.R. Mirasso, Opt. Lett. **36**, 2212 (2011)
12. M.C. Soriano, L. Zunino, O.A. Rosso, I. Fischer, C.R. Mirasso, IEEE J. Quantum Electron. **47**, 252 (2011)
13. L. Zunino, M.C. Soriano, I. Fischer, O.A. Rosso, C.R. Mirasso, Phys. Rev. E **82**, 046212 (2010)
14. L. Zunino, M.C. Soriano, O.A. Rosso, Phys. Rev. E **86**, 046210 (2012)
15. O.A. Rosso, L.C. Carpi, P.M. Saco, M. Gómez Ravetti, A. Plastino, H.A. Larrondo, Physica A **391**, 42 (2012)
16. O.A. Rosso, L.C. Carpi, P.M. Saco, M. Gómez Ravetti, H.A. Larrondo, A. Plastino, Eur. Phys. J. B **85**, 419 (2012)
17. J.M. Amigó, L. Kocarev, J. Szczepanski, Phys. Lett. A **355**, 27 (2006)
18. J.M. Amigó, S. Zambrano, M.A.F. Sanjuán, Europhys. Lett. **83**, 60005 (2008)
19. L.C. Carpi, P.M. Saco, O.A. Rosso, Physica A **389**, 2020 (2010)
20. H. Wold, *A Study in the Analysis of Stationary Time Series* (Almqvist and Wiksell, Upsala, 1938)
21. J. Kurths, H. Herzel, Physica D **25**, 165 (1987)
22. S. Cambanis, C.D. Hardin, A. Weron, Probab. Theory Related Fields **79**, 1 (1988)
23. D.P. Feldman, J.P. Crutchfield, Phys. Lett. A **238**, 244 (1998)
24. D.P. Feldman, C.S. McTague, J.P. Crutchfield, Chaos **18**, 043106 (2008)
25. P.W. Lamberti, M.T. Martín, A. Plastino, O.A. Rosso, Physica A **334**, 119 (2004)
26. R. López-Ruiz, H.L. Mancini, X. Calbet, Phys. Lett. A **209**, 321 (1995)
27. C. Shannon, W. Weaver, *The Mathematical theory of communication* (University of Illinois Press, Champaign, 1949)
28. I. Grosse, P. Bernaola-Galván, P. Carpena, R. Román-Roldán, J. Oliver, H.E. Stanley, Phys. Rev. E **65**, 041905 (2002)
29. A.R. Plastino, A. Plastino, Phys. Rev. E **54**, 4423 (1996)
30. M.T. Martín, A. Plastino, O.A. Rosso, Physica A **369**, 439 (2006)
31. O.A. Rosso, L. De Micco, H. Larrondo, M.T. Martín, A. Plastino, Int. J. Bifur. Chaos **20**, 775 (2010)
32. L. Zunino, M. Zanin, B.M. Tabak, D.G. Pérez, O.A. Rosso, Physica A **389**, 1891 (2010)
33. L. Zunino, B.M. Tabak, F. Serinaldi, M. Zanin, D.G. Pérez, O.A. Rosso, Physica A **390**, 876 (2011)
34. L. Zunino, A. Fernández Bariviera, M.B. Guercio, L.B. Martinez, O.A. Rosso, Physica A **391**, 4342 (2012)
35. J.C. Sprott, *Chaos and time series analysis* (Oxford University Press, New York, 2003)
36. R. May, Nature **261**, 45 (1976)
37. S.H. Strogatz, *Nonlinear dymanics and chaos with applications to physics, biology, chemistry, and engineering* (Addison-Wesley-Longman, Reading, 1994)
38. R.L. Devaney, *An introduction to chaotic dynamical systems*, 2nd edn. (Addison-Wesley, Redwood City, 1989)
39. D.E. Knuth, *Sorting and searching, Vol. 3 of The art of computer programming*, 3rd edn. (Addison-Wesley-Longman, Reading, 1997)

40. W. Zeng, M. Ding, J. Li, Chinese Phys. Lett. **2**, 293 (1985)
41. W. Ricker, J. Fish. Res. Board Canada **11**, 559 (1954)
42. M.A. van Wyk, W. Steeb, *Chaos in electronics* (Kluwer, Dordrecht, 1997)
43. C. Beck, F. Schlögl, *Thermodynamics of chaotics systems* (Cambridge University Press, New York, 1995)
44. A. Potapov, M.K. Ali, Phys. Lett. A **277**, 310 (2000)
45. R. Shaw, Z. Naturforsch. A **36**, 80 (1981)
46. V.I. Arnold, Am. Math. Soc. Transl. Ser. **46**, 213 (1965)
47. M. Hénon, Commun. Math. Phys. **50**, 69 (1976)
48. R. Lozi, J. Phys. **39**, 9 (1978)
49. D.G. Aronson, M.A. Chory, G.R. Hall, R.P. McGehee, Commun. Math. Phys. **83**, 304 (1982)
50. H.E. Nusse, J.A. Yorke, *Dynamics: numerical explorations* (Springer, New York, 1994)
51. R.R. Whitehead, N. Macdonald, Physica D **13**, 401 (1984)
52. P.J. Holmes, Philos. Trans. Roy. Soc. London Ser. A **292**, 419 (1979)
53. G. Schmidt, B.H. Wang, Phys. Rev. A **32**, 2994 (1985)
54. E. Ikeda, Opt. Commun. **30**, 257 (1979)
55. Ya. G. Sinai, Russian Math. Surv. **27**, 21 (1972)
56. J.R. Beddington, C.A. Free, J.H. Lawton, Nature **255**, 58 (1975)
57. B.V. Chirikov, Phys. Rep. **52**, 273 (1979)
58. M. Hénon, Quart. Appl. Math. **27**, 291 (1969)
59. V.I. Arnold, A. Avez, *Ergodic problems of classical mechanics* (Benjamin, New York, 1968)
60. R.L. Devaney, Physica D **10**, 387 (1984)
61. A.A. Chernikov, R.Z. Sagdeev, G.M. Zaslavsky, Phys. Today **41**, 27 (1988)
62. E.N. Lorenz, *The essence of chaos* (University of Washington Press, Seattle, 1993)
63. B. Nagy, J.D. Farmer, J.E. Trancik, J.P. Gonzales, Technol. Forecast. Soc. Change **78**, 1356 (2011)
64. H.A. Larrondo, Matlab program: *noisefk.m* (2012), http://www.mathworks.com/matlabcentral/fileexchange/35381
65. S.I. Resnick, *A Probability Path* (Birkhäuser, Boston, 1999)
66. C.F. Manski, *Analog estimation methods in econometrics*, in *Monographs on Statistics and Applied Probability* (Chapman & Hall, New York, 1988), Vol. 39